

Article

Nanoporous Sodium Carboxymethyl Cellulose-g-poly (Sodium Acrylate)/FeCl₃ Hydrogel Beads: Synthesis and Characterization

Bijender Kumar ^{1,2}, Ruchir Priyadarshi ³ , Sauraj ⁴, Farha Deeba ¹, Anurag Kulshreshtha ⁵, Kirtiraj K. Gaikwad ⁵, Jaehwan Kim ² , Anuj Kumar ^{6,*} and Yuvraj Singh Negi ^{1,*}

- ¹ Department of Polymer and Process Engineering, Indian Institute of Technology Roorkee, Roorkee 247667, India; bijenderkumarchem@gmail.com (B.K.); farha.deeba86@gmail.com (F.D.)
- ² Creative Research Center for Nanocellulose Future Composites, Department of Mechanical Engineering, Inha University, Inharo, Michuhol-gu, Incheon 22212, Korea; jaehwan@inha.ac.kr
- ³ Department of Food and Nutrition, Bio Nanocomposite Research Center, Kyung Hee University, Seoul 02447, Korea; ruchirpriyadarshi@gmail.com
- ⁴ Department of Materials Engineering, Indian Institute of Science, Bangalore 560012, India; saurajpolymeriitd@gmail.com
- ⁵ Department of Paper Technology, Indian Institute of Technology Roorkee, Roorkee 247667, India; anuragk77@gmail.com (A.K.); gaikwad.msu@gmail.com (K.K.G.)
- ⁶ School of Chemical Engineering, Yeungnam University, Gyeongsan 38541, Korea
- * Correspondence: anuj.budhera@gmail.com (A.K.); yuvrajnegi@gmail.com (Y.S.N.)

Received: 24 November 2020; Accepted: 9 December 2020; Published: 11 December 2020



Abstract: Novel sodium carboxymethyl cellulose-g-poly (sodium acrylate)/Ferric chloride (CMC-g-PNaA/FeCl₃) nanoporous hydrogel beads were prepared based on the ionic cross-linking between CMC-g-PNaA and FeCl₃. The structure of CMC and CMC-g-PNaA were elucidated by Fourier transform infrared spectroscopy (FTIR) and nuclear magnetic resonance (NMR) spectroscopy, and the elemental composition was analyzed by energy dispersive X-ray analysis (EDX). The physicochemical properties of the CMC-g-PNaA/FeCl₃ hydrogel beads were analyzed by X-ray diffraction (XRD), scanning electron microscopy (SEM), atomic force microscopy (AFM) and thermogravimetric analysis (TGA). The swelling percentage of hydrogel beads was studied at different time periods. The obtained CMC-g-PNaA/FeCl₃ hydrogel beads exhibited a higher nanoporous morphology than those of CMC-g-PNaA and CMC beads. Furthermore, an AFM image of the CMC-g-PNaA/FeCl₃ beads shows granule type topology. Compared to the CMC-g-PNaA (189 °C), CMC-g-PNaA/FeCl₃ hydrogel beads exhibited improvement in thermal stability (199 °C). Furthermore, CMC-g-PNaA/FeCl₃ hydrogel beads depicted a higher swelling percentage capacity of around 1452%, as compared to CMC-g-PNaA (1096%). Moreover, this strategy with preliminary results could be useful for the development of polysaccharide-based hybrid hydrogel beads for various potential applications.

Keywords: sodium carboxymethyl cellulose; poly(sodium acrylate); FeCl₃; cross-linking; nanoporous beads; hydrogel; thermal analysis

1. Introduction

Hydrogels are three-dimensional polymeric network structures with a higher capacity to absorb water due to the presence of hydrophilic groups, but which are insoluble in water. Hydrogels are gaining significant attention of the researchers due to their application in various research fields, such as wastewater treatment, agriculture, tissue engineering, drug delivery and electroactive applications [1–4]. Currently, researchers have focused on the development of polysaccharide-based hydrogels due to

their cost effectiveness, biodegradability and higher ability to remove pollutants as compared to synthetic polymeric hydrogels [5–7]. As polysaccharide, sodium carboxymethyl cellulose (CMC) is a high-molecular weight anionic polymeric material that contains numerous hydroxyl ($-\text{OH}$) and carboxylate ($-\text{COO}^-$) groups [8]. Due to its biodegradability, biocompatibility and non-toxicity, it has been extensively used in tissue engineering, drug delivery, textile industry, paper, dispersant and water treatment applications [1,9–11].

Thus far, few polysaccharide-based hydrogel beads including alginate [12], CMC/dextran sulfate [13], calcium alginate-CMC [14], CMC-NPS [15], sodium alginate-CMC [16], alginate/ Ca^{2+} [17], silsesquioxane/CMC [8] and cellulose nanocrystal/sodium alginate [18] have been developed with improved properties. In addition, Yanshu Shi et al. have reported the porous organic polymeric network and used it for the photothermal therapy, which was prepared by the metalation of polymers with Fe^{3+} ions [19,20]. Yang and co-workers reported CMC hydrogel beads that were prepared by the cross-linking of epichlorohydrin with CMC. The hydrogel beads showed the capability to adsorb toxic metals [21]. Agarwal et al. developed CMC-based hydrogel beads by ionic-gelation methods for drug delivery systems [14]. Similarly, Ren and co-workers developed the CMC gel-based beads via blending, followed by cross-linking, and also studied the effect of pH, temperature and dosage of beads on the adsorption behavior of Pb^{2+} [16]. Furthermore, Akalin and Pulat have reported cross-linked CMC hydrogel beads prepared by cross-linking between CMC chains with ferric chloride (FeCl_3) as a cross-linker, and investigated the pore size, swelling and degradation behavior [22]. Recently, CMC/zinc oxide (ZnO)-based nanocomposite hydrogel was developed by the ionic cross-linking of CMC with Zn^{2+} ions. The cross-linked nanocomposite hydrogel showed high swelling properties and strong antimicrobial activity, which could be used in biomedical and superabsorbent applications [23].

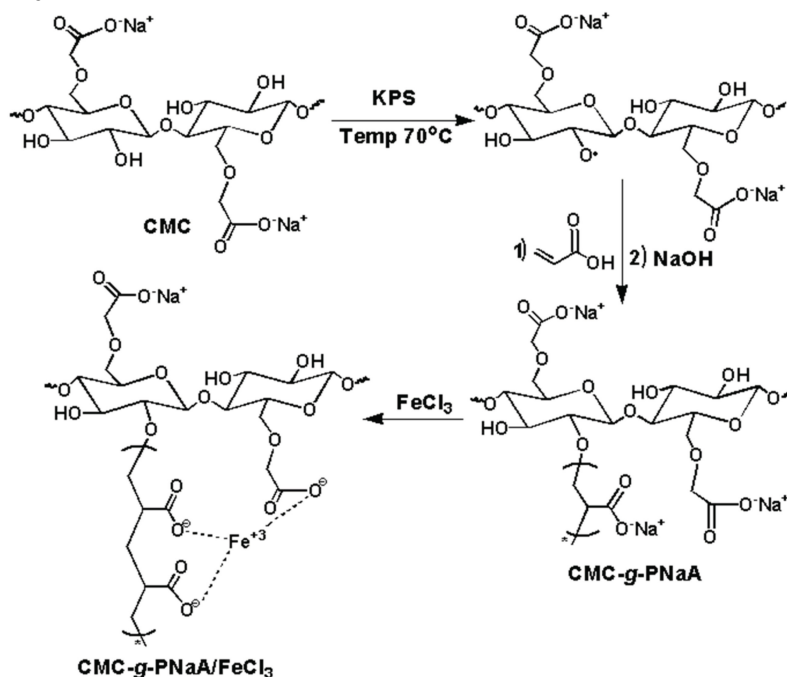
In recent years, several studies have been undertaken in hydrogel materials of acrylic acid (AA)-grafted polysaccharides, namely CMC-g-PAA [24], chitosan/PAA [25], PAA-hydroxyethyl cellulose [26], Amylose-g-PAA [27] and various AA-grafted polysaccharides [28,29] for superabsorbent, waste water treatment and biomedical applications. Until now, ionically cross-linked nanoporous hydrogel beads of CMC-g-poly (sodium acrylate) (PNaA) have not been reported. In this work, we introduced the novel nanoporous CMC-g-PNaA/ FeCl_3 hydrogel beads that were developed by the ionic cross-linking of CMC-g-PNaA in the presence of FeCl_3 as an ionic cross-linker, while CMC-g-PNaA was synthesized by the grafting of AA onto CMC in the presence of potassium persulfate initiator. In this study, the effect of ionic linkage on the thermal stability, pore size and swelling behavior of CMC-g-PNaA/ FeCl_3 hydrogel beads was investigated.

2. Results and Discussion

2.1. Structural Characterization

Ionic cross-linked CMC-g-PNaA/ FeCl_3 hydrogel beads were prepared by the cross-linking of CMC-g-PNaA, followed by the grafting polymerization of AA onto CMC, as shown in Scheme 1. The homopolymer could be formed during the polymerization, but it may be mostly dissolved during the precipitation of reaction mixture. Cross-linked CMC-g-PNaA/ FeCl_3 hydrogel beads were formed by the intra-molecular interaction of ionic metals with CMC-g-PNaA chains. Nevertheless, inter-molecular cross-linking might be induced by the interaction of ionic metals with CMC-g-PNaA and the remaining content of the homopolymer [30]. In Figure 1, as reported in literature [1,31–33], CMC depicts the Fourier transform infrared spectroscopy (FTIR) absorption band at 1590 cm^{-1} and 1420 cm^{-1} ascribed to the carboxylate groups, which are a characteristic band from CMC (Figure 1). The broad absorption bands at around 3418 cm^{-1} are attributed to the $-\text{OH}$ stretching, while the band 2920 cm^{-1} corresponds to C–H stretching. Furthermore, the bands between $1000\text{--}1200\text{ cm}^{-1}$ are attributed to the C–O stretching [34]. In the FTIR of CMC-g-PNaA, the band intensities of C–H stretching at 2920 cm^{-1} and carboxylate group at 1590 cm^{-1} and 1420 cm^{-1} were increased after the grafting of neutralized AA onto CMC [35], which confirms the successful formation of CMC-g-PNaA.

Furthermore, in case of CMC-g-PNaA/FeCl₃, a new band at 1745 cm⁻¹ appeared due to the electrostatic interaction between CMC-g-PNaA and Fe³⁺ ions [22]. This new band confirms the formation of ionic cross-linked CMC-g-PNaA/FeCl₃. Moreover, all absorption bands of CMC (3418, 2920, 1590, 1420, 1329 and 1200–1000 cm⁻¹) and CMC-g-PNaA (3418, 2920, 1605, 1420, 1329 and 1061 cm⁻¹) are visible in the ionic cross-linked CMC-g-PNaA/FeCl₃. The absorption bands of CMC in the spectrum of CMC-g-PNaA/FeCl₃ are similar with the cellulose skeleton.



Scheme 1. Schematic presentation of ionic cross-linked CMC-g-PNaA/FeCl₃.

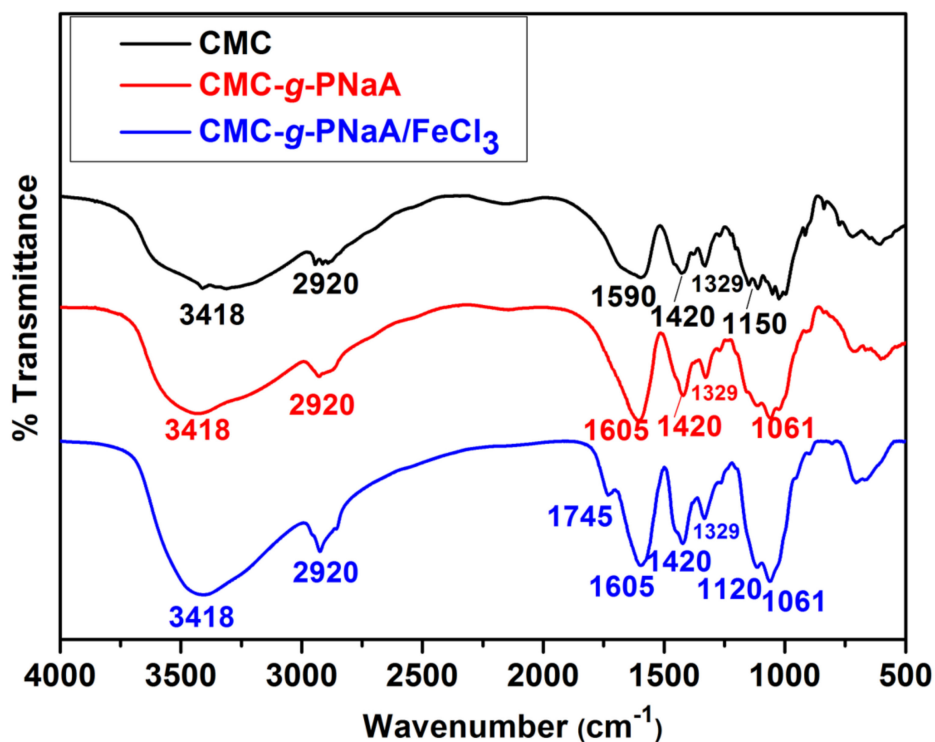


Figure 1. Fourier transform infrared spectroscopy (FTIR) of CMC, CMC-g-PNaA and CMC-g-PNaA/FeCl₃.

Furthermore, nuclear magnetic resonance (NMR) spectroscopy was employed to characterize the CMC and CMC-*g*-PNaA. CMC showed characteristic signals in the region of 3.0 ppm to 4.3 ppm (Figure 2). Moreover, the new characteristic signals appeared in the NMR spectra of CMC-*g*-PNaA in the regions of 1.11–1.93 ppm and 1.97–2.88 ppm, which were obtained due to the $-\text{CH}_2^{\text{a}}$ - and $-\text{CH}^{\text{b}}$ - of PAA content (Figure 2) [35,36] and confirms the successful formation of CMC-*g*-PNaA. In addition, the successful grafting of CMC-*g*-PNaA copolymer and its effective ionic-crosslinking with Fe^{3+} ions was confirmed by energy dispersive X-ray analysis (EDX) spectra, as shown in Figure 3. CMC-*g*-PNaA exhibited increased content of carbon and oxygen elements than that of only CMC. Here, the peak intensity of the C and O elements was increased, which demonstrated a successful grafting of CMC and PNaA. Furthermore, in EDX spectra of CMC-*g*-PNaA/ FeCl_3 , a new peak of the Fe element emerged, and the peak intensity of the Na element was significantly decreased after the ionic-crosslinking of CMC-*g*-PNaA with Fe^{3+} ions. This indicates the effective ionic-crosslinking between Fe^{3+} ions and polymeric chains (see Scheme 1).

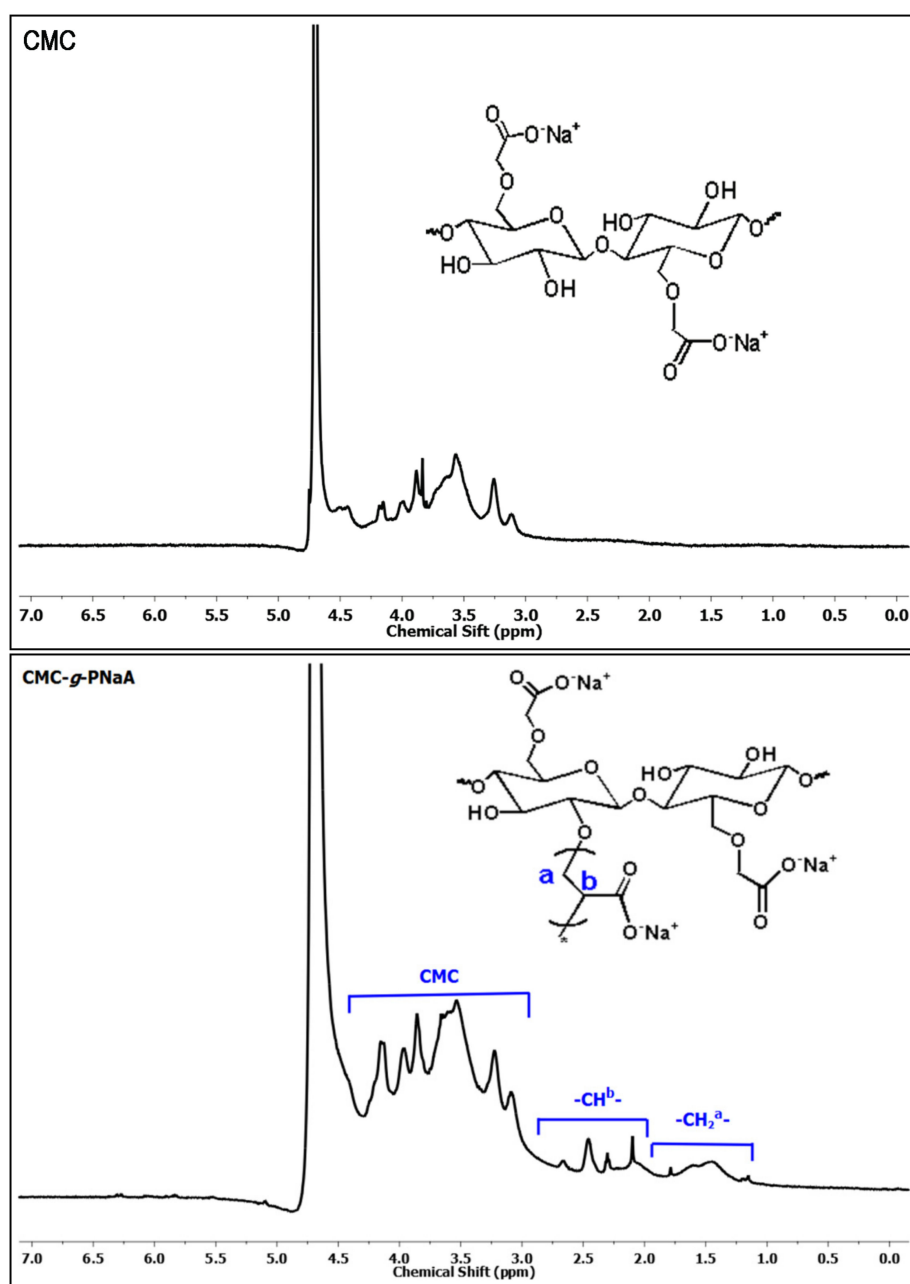


Figure 2. ^1H nuclear magnetic resonance (NMR) spectrum of CMC and CMC-*g*-PNaA.

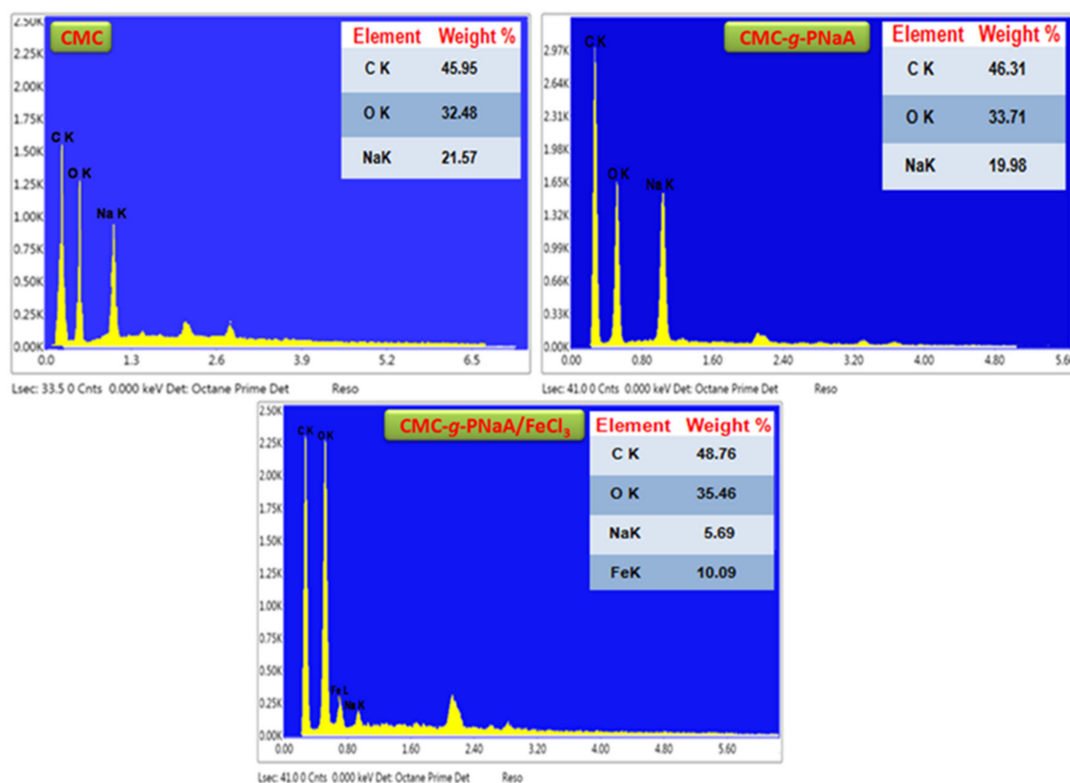


Figure 3. Energy dispersive X-ray analysis (EDX) spectra of CMC, CMC-g-PNaA and CMC-g-PNaA/FeCl₃ hydrogel beads.

X-ray diffraction (XRD) patterns of CMC show the characteristic peaks at $2\theta = 20.76^\circ$, 31.84° and 45.48° , which indicate the amorphous and crystalline structure. Furthermore, CMC-g-PNaA shows broad peaks at around 22.46° and 32.15° , which demonstrate that the crystalline region of CMC is destroyed after grafting of AA onto CMC. Meanwhile, CMC-g-PNaA/FeCl₃ depicts a broad peak with two small intense peaks at around 27.15° and 35.24° , due to the ionic cross-linking of CMC-g-PNaA with Fe³⁺ ions, as shown in Figure 4 [37]. After ionic cross-linking, the XRD peaks of CMC-g-PNaA were shifted from the lower to higher 2θ values, which indicate the successful ionic cross-linking of Fe³⁺ with CMC-g-PNaA chains.

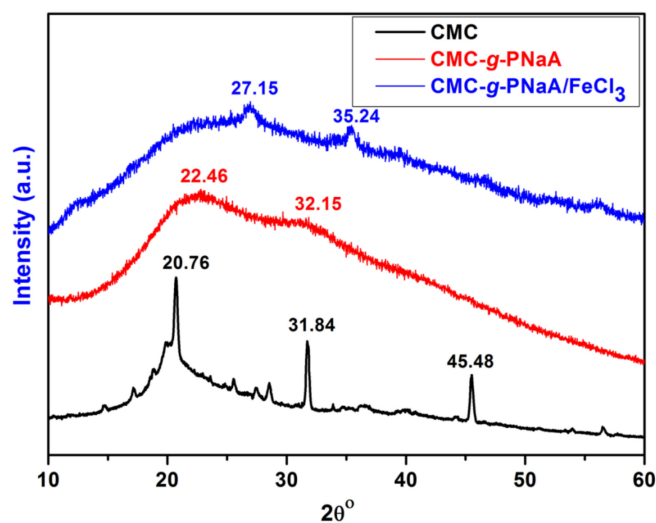


Figure 4. X-ray diffraction (XRD) patterns of CMC, CMC-g-PNaA and CMC-g-PNaA/FeCl₃ hydrogel beads.

2.2. Thermal Gravimetric Analysis (TGA)

Compared to the CMC and CMC-g-PNaA, CMC-g-PNaA/FeCl₃ exhibits the one step degradation (Figure 5). In CMC, the major decomposition started at 240 °C, with 14.34% weight loss due to inorganic moiety, including minor weight (4.61%) loss from 154 °C to 202 °C. Moreover, the decomposition after 335 °C occurred due to the pyrolysis reaction [1]. Below 120 °C, the minor weight loss in all samples occurred due to the loss of moisture. CMC-g-PNaA shows the continued degradation up to 189 °C with 11.47% weight loss, which may be attributed to the desorbed water. Afterwards, the major degradation occurred from 189 °C to 400 °C with 48.94% weight loss, which may be attributed to the degradation of the side group and chain scission. The last degradation appeared after 400 °C with 27.35% weight loss, due to the pyrolysis reaction and chain scission [35]. Furthermore, CMC-g-PNaA/FeCl₃ demonstrated initial degradation at 199 °C with 9.6% weight loss due to the moisture. After that, the main degradation was attributed up to 472 °C with 66.37% weight loss, which may be occurred due to side group scission, side chain scission and pyrolysis degradation of the CMC unit. Moreover, CMC-g-PNaA/FeCl₃ reveals the higher residue of around 23% than those of CMC (15%) and CMC-g-PNaA (12%), as shown in (Figure 5a). Thermogravimetric analysis (TGA) results demonstrate that CMC-g-PNaA/FeCl₃ exhibits higher thermal stability of 199 °C. The thermal stability of CMC-g-PNaA/FeCl₃ is comparable with the previously reported literature of grafted-based polysaccharides hydrogel [38,39].

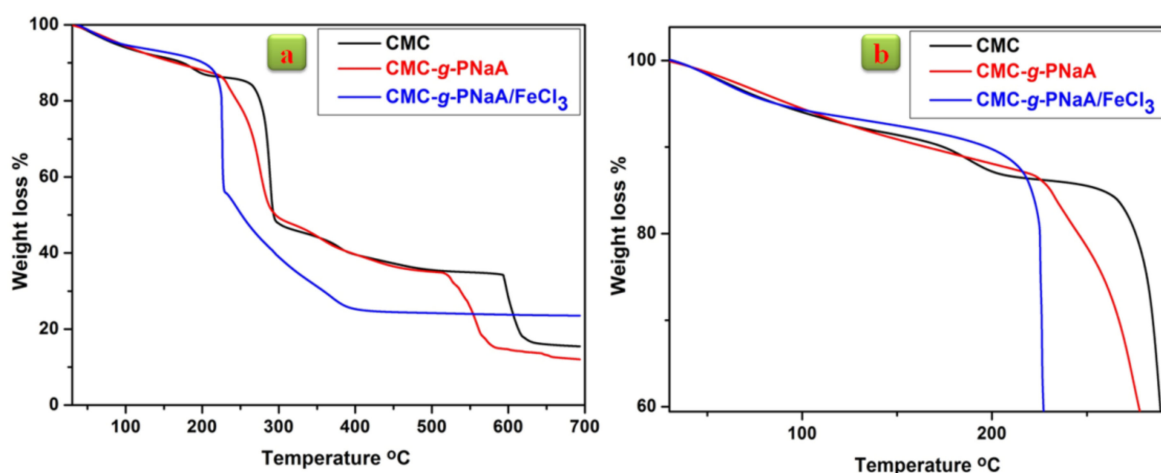


Figure 5. (a) Thermogravimetric analysis (TGA) curves of CMC, CMC-g-PNaA CMC-g-PNaA/FeCl₃; and their corresponding (b) extended TGA curves.

2.3. Morphological Analysis

The surface morphology of CMC, CMC-g-PNaA and CMC-g-PNaA/FeCl₃ hydrogel beads was analyzed by scanning electron microscopy (SEM) (Figure 6). CMC shows the crystalline and fiber type morphology (Figure 6a), while CMC-g-PNaA exhibits a porous morphology. The SEM results demonstrate that when AA was grafted onto CMC, the morphology was converted to porous with a different size and shape from crystalline and fiber-type morphology (Figure 6b). Moreover, CMC-g-PNaA/FeCl₃ hydrogel beads depict the dense irregular-sized porous morphology as compared to the CMC-g-PNaA. Here, CMC-g-PNaA/FeCl₃ showed the minimum and maximum pore size as around 66 nm and 800 nm, as were measured by ImageJ Software. Despite the large size of some pores (around 800 nm), the average pore size of CMC-g-PNaA/FeCl₃ hydrogel beads was obtained at around 280 nm (Figure 6c). In addition, Figure 6d shows the atomic force microscopy (AFM) image of CMC-g-PNaA/FeCl₃ hydrogel beads, and it indicates the granular topology of the obtained hydrogel beads (Figure 6e). Therefore, AFM analysis depicts the homogenous granular morphology of CMC-g-PNaA/FeCl₃ hydrogel beads. The average surface roughness (R_a) and root mean square roughness (R_{ms}) of beads were obtained to be 10.8 nm and 107 nm, respectively.

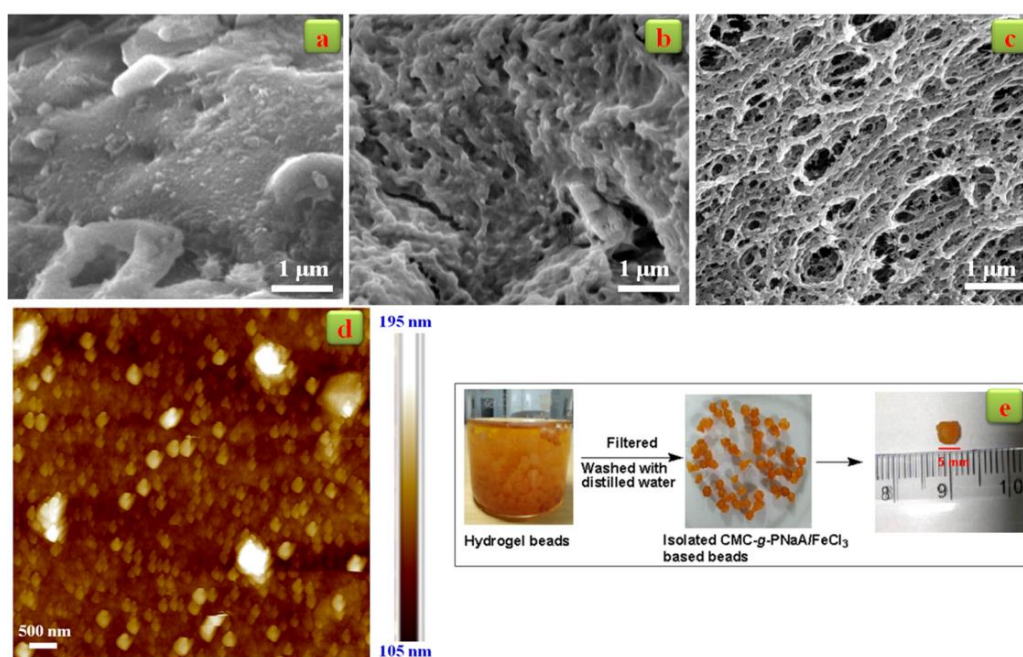


Figure 6. Scanning electron microscopy (SEM) images of (a) CMC; (b) CMC-g-PNaA; and (c) CMC-g-PNaA/FeCl₃; (d) atomic force microscopy (AFM) image of CMC-g-PNaA/FeCl₃ hydrogel bead; and (e) isolated beads of CMC-g-PNaA/FeCl₃.

2.4. Swelling Study

The swelling behavior of CMC-g-PNaA and CMC-g-PNaA/FeCl₃ hydrogel beads is shown in Figure 7 as a function of time. It was found that the swelling rate of ionic cross-linked CMC-g-PNaA/FeCl₃ hydrogel beads is initially very high, but after 8 h, the hydrogel beads reached the equilibrium swelling rate. CMC-g-PNaA/FeCl₃ hydrogel beads showed the highest swelling rate of up to 1452% in the time range of 10 h to 12 h. In addition, the swelling rate of CMC-g-PNaA increased gradually with time up to 6 h, while it started to decrease after 10 h due to the breaking of the polymeric chain. CMC-g-PNaA exhibits the equilibrium swelling rate as around 1096% [38]. Moreover, the higher swelling percentage of CMC-g-PNaA/FeCl₃ may be attributed to the higher porosity of hydrogel beads. The higher swelling rate of CMC-g-PNaA/FeCl₃ exhibits as compared to CMC-g-PNaA may be attributed to the ionic cross-linking, resulting in a higher number of pores with a greater pore size as compared to the CMC-g-PNaA.

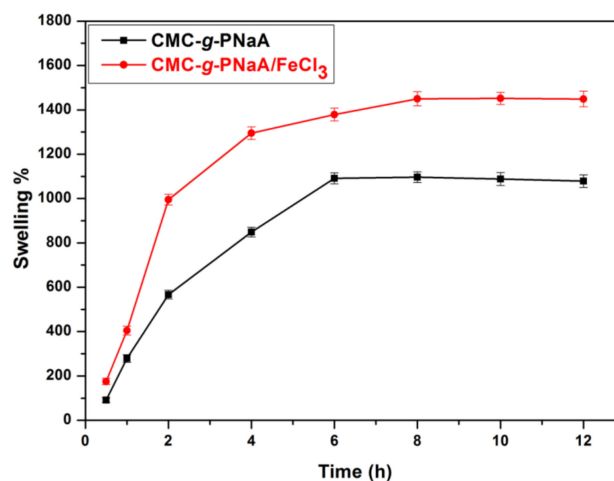


Figure 7. Swelling behavior of CMC-g-PNaA and CMC-g-PNaA/FeCl₃ hydrogel beads.

3. Conclusions

In this study, novel CMC-g-PNaA/FeCl₃ hydrogel beads were prepared based on ionic-interactions between CMC-g-PNaA and FeCl₃ as an ionic-crosslinker. TGA demonstrated that the CMC-g-PNaA/FeCl₃ hydrogel beads showed higher thermal stability at around 199 °C as compared to CMC-g-PNaA, which was stable up to 189 °C. CMC-g-PNaA/FeCl₃ hydrogel beads showed higher pore density with an average pore size of 280 nm. Furthermore, AFM images revealed the granule type topology of beads with $R_a = 10.8$ nm. CMC-g-PNaA/FeCl₃ hydrogel beads showed a swelling percentage of 1452% as compared to 1096% for CMC-g-PNaA. Overall, the ionic linkage between CMC-g-PNaA and FeCl₃ significantly improved the physical properties of the hydrogel, and the obtained CMC-g-PNaA/FeCl₃ hydrogel beads could have potential applications in waste water treatment and agriculture.

4. Materials and Methods

4.1. Materials

CMC (low viscosity; 50–200 cP) was procured from Sigma Aldrich (Bangalore, India). AA $\geq 99\%$, FeCl₃ $\geq 98\%$, Sodium hydroxide (NaOH, $\geq 98\%$) and Acetone and Potassium persulfate (KPS, $\geq 99\%$) were procured from Hi-Media (Mumbai, India). All the materials were used as received, without any purification.

4.2. Synthesis of CMC-g-PNaA

CMC-g-PNaA was synthesized by the following procedure [38,40]: firstly, 1.0 g of CMC was dissolved in 50 mL distilled water for 1 h at room temperature, and an inert atmosphere in a three neck flask equipped with a magnetic stirrer. Following this, KPS (0.2 g) initiator was added into the CMC solution at 70 °C, and after 30 min, neutralized AA (3.5 mL) was inserted into the reaction mixture and heated for 2 h. Thereafter, the pH of the reaction mixture was raised up to 8 by using a NaOH solution, and the mixture was precipitated by acetone. Finally, CMC-g-PNaA precipitate was collected and dried in a vacuum oven for 24 h at 60 °C.

4.3. Preparation of CMC-g-PNaA/FeCl₃ Hydrogel Beads

CMC-g-PNaA/FeCl₃ hydrogel beads were prepared by the following procedure [22]: firstly, CMC-g-PNaA (2% w/v) was dissolved in distilled water by using a mechanical stirrer at 300 rpm for 6 h. Then, 50 mL of CMC-g-PNaA solution was added dropwise in the 100 mL aqueous solution of FeCl₃ (0.020 mol). After that, the obtained spherical hydrogel beads were filtered, washed with distilled water and dried in vacuum oven for 24 h.

4.4. Characterization

FT-IR spectra of the CMC, CMC-g-PNaA and CMC-g-PNaA/FeCl₃ were recorded using FT-IR spectroscopy (Perkin Elmer FT-IR C91158 Spectrum, Waltham, MA, USA) within the range of 4000 cm⁻¹ to 500 cm⁻¹.

¹H-NMR spectra of CMC and CMC-g-PNaA was obtained in D₂O solvent with the help of a NMR spectrometer (Bruker 500 MHz, Rheinstetten, Germany).

The elemental analysis of CMC, CMC-g-PNaA and CMC-g-PNaA/FeCl₃ was analyzed by the EDX (Mira 3 Tescan, Kohoutovice, Czech Republic) instrument.

XRD spectra were obtained using a Rigaku Ultima IV diffractometer (Tokyo, Japan) equipped with a Cu-K α radiation ($\lambda = 0.154$ nm) in the 2θ range of 5°–60°, with a voltage of 40 kV and a current of 40 mA.

The thermal stability of the CMC, CMC-g-PNaA and CMC-g-PNaA/FeCl₃ was analyzed by TGA using Exstar TGA/DTG 6300 (Tokyo, Japan) at a 10 °C min⁻¹ heating rate in the presence of nitrogen (flow rate: 200 mL/min).

The hydrogel surface morphology and pore size of CMC-g-PNaA/FeCl₃, along with CMC and CMC-g-PNaA, was evaluated by a SEM (Mira 3 Tescan, Kohoutovice, Czech Republic) instrument. Topographical analysis of CMC-g-PNaA/FeCl₃ was performed by Bruker Dimension Icon Atomic Force Microscope, USA.

The swelling % of CMC-g-PNaA and CMC-g-PNaA/FeCl₃ hydrogel beads was performed at room temperature with the help of tea-bag methods as a function of time. For this, dried hydrogel beads (0.02 g) were added to clean empty tea-bags and immersed in 100 mL water. Furthermore, swollen hydrogel beads were taken out at regular time intervals, and after that the weight was measured. The swelling behavior (%) was determined as follows [41]:

$$\text{Swelling \%} = \frac{(W_2 - W_1)}{W_1} \times 100$$

where W_1 is the weight of the dried hydrogel bead, while the W_2 is the weight of the swollen hydrogel bead.

Author Contributions: Conceptualization, B.K.; methodology, B.K.; formal analysis and investigation, B.K., R.P., S. and F.D.; writing—original draft preparation, B.K.; writing—review and editing, A.K. (Anurag Kulshreshtha), K.K.G., J.K., A.K. (Anuj Kumar) and Y.S.N.; and supervision, A.K. (Anuj Kumar) and Y.S.N. All authors have read and agreed to the published version of the manuscript.

Funding: This research received no external funding.

Acknowledgments: Authors would like to acknowledge the IIT Roorkee for the financial support and facilities in carrying out this research work.

Conflicts of Interest: The authors declare no conflict of interest.

References

1. Kumar, B.; Negi, Y.S. To investigate the effect of ester-linkage on the properties of polyvinyl alcohol/carboxymethyl cellulose based hydrogel. *Mater. Lett.* **2019**, *252*, 308–312. [[CrossRef](#)]
2. Kumar, B.; Deeba, F.; Priyadarshi, R.; Sauraj, R.; Bano, S.; Kumar, A.; Negi, Y.S. Development of novel cross-linked carboxymethyl cellulose/poly(potassium 1-hydroxy acrylate): Synthesis, characterization and properties. *Polym. Bull.* **2019**. [[CrossRef](#)]
3. Jayaramudu, T.; Ko, H.U.; Kim, H.C.; Kim, J.W.; Li, Y.; Kim, J. Transparent and semi-interpenetrating network P(vinyl alcohol)-P(Acrylic acid) hydrogels: pH responsive and electroactive application. *Int. J. Smart Nano Mater.* **2017**, *8*, 80–94. [[CrossRef](#)]
4. Kumar, A.; Rao, K.M.; Han, S.S. Mechanically viscoelastic nanoreinforced hybrid hydrogels composed of polyacrylamide, sodium carboxymethylcellulose, graphene oxide, and cellulose nanocrystals. *Carbohydr. Polym.* **2018**, *193*, 228–238. [[CrossRef](#)] [[PubMed](#)]
5. Qi, X.; Wu, L.; Su, T.; Zhang, J.; Dong, W. Polysaccharide-based cationic hydrogels for dye adsorption. *Colloids Surf. B Biointerfaces* **2018**, *170*, 364–372. [[CrossRef](#)]
6. Yuan, Z.; Wang, J.; Wang, Y.; Liu, Q.; Zhong, Y.; Wang, Y.; Li, L.; Lincoln, S.F.; Guo, X. Preparation of a poly(acrylic acid) based hydrogel with fast adsorption rate and high adsorption capacity for the removal of cationic dyes. *RSC Adv.* **2019**, *9*, 21075–21085. [[CrossRef](#)]
7. Elbedwehy, A.M.; Atta, A.M. Novel superadsorbent highly porous hydrogel based on arabic gum and acrylamide grafts for fast and efficient methylene blue removal. *Polymers* **2020**, *12*, 338. [[CrossRef](#)]
8. Liu, H.; Huang, S.; Li, X.; Zhang, L.; Tan, Y.; Wei, C.; Lv, J. Facile fabrication of novel polyhedral oligomeric silsesquioxane/carboxymethyl cellulose hybrid hydrogel based on supermolecular interactions. *Mater. Lett.* **2013**, *90*, 142–144. [[CrossRef](#)]
9. Ninan, N.; Muthiah, M.; Park, I.; Kalarikkal, N.; Elain, A.; Wui, T.; Thomas, S.; Grohens, Y. Wound healing analysis of pectin/carboxymethyl cellulose/micro fi brillated cellulose based composite scaffolds. *Mater. Lett.* **2014**, *132*, 34–37. [[CrossRef](#)]

10. Salahinejad, E.; Hadianfard, M.J.; MacDonald, D.D.; Mozafari, M.; Vashae, D.; Tayebi, L. Zirconium titanate thin film prepared by an aqueous particulate sol-gel spin coating process using carboxymethyl cellulose as dispersant. *Mater. Lett.* **2012**, *88*, 5–8. [[CrossRef](#)]
11. Tiwari, N.; Nawale, L.; Sarkar, D.; Badiger, M. Carboxymethyl Cellulose-Grafted Mesoporous Silica Hybrid Nanogels for Enhanced Cellular Uptake and Release of Curcumin. *Gels* **2017**, *3*, 8. [[CrossRef](#)] [[PubMed](#)]
12. Kühbeck, D.; Mayr, J.; Häring, M.; Hofmann, M.; Quignard, F.; Díaz Díaz, D. Evaluation of the nitroaldol reaction in the presence of metal ion-crosslinked alginates. *New J. Chem.* **2015**, *39*, 2306–2315. [[CrossRef](#)]
13. Benhalima, T.; Ferfera-Harrar, H. Eco-friendly porous carboxymethyl cellulose/dextran sulfate composite beads as reusable and efficient adsorbents of cationic dye methylene blue. *Int. J. Biol. Macromol.* **2019**, *132*, 126–141. [[CrossRef](#)] [[PubMed](#)]
14. Agarwal, T.; Hari, S.N.G.; Pal, K.; Pramanik, K.; Giri, S.; Banerjee, I. Macromolecules Calcium alginate-carboxymethyl cellulose beads for colon-targeted drug delivery. *Int. J. Biol. Macromol.* **2015**, *75*, 409–417. [[CrossRef](#)] [[PubMed](#)]
15. Uva, M.; Mencuccini, L.; Atrei, A.; Innocenti, C.; Fantechi, E.; Sangregorio, C.; Maglio, M.; Fini, M.; Barbucci, R. On the Mechanism of Drug Release from Polysaccharide Hydrogels Cross-Linked with Magnetite Nanoparticles by Applying Alternating Magnetic Fields: The Case of DOXO Delivery. *Gels* **2015**, *1*, 24–43. [[CrossRef](#)]
16. Ren, H.; Gao, Z.; Wu, D.; Jiang, J.; Sun, Y.; Luo, C. Efficient Pb (II) removal using sodium alginate—carboxymethyl cellulose gel beads: Preparation, characterization, and adsorption mechanism. *Carbohydr. Polym.* **2016**, *137*, 402–409. [[CrossRef](#)]
17. Yamamoto, K.; Yuguchi, Y.; Stokke, B.T.; Sikorski, P.; Bassett, D.C. Local structure of Ca²⁺ alginate hydrogels gelled via competitive ligand exchange and measured by small angle X-ray scattering. *Gels* **2019**, *5*, 3. [[CrossRef](#)]
18. Hu, Z.H.; Omer, A.M.; Ouyang, X.K.; Yu, D. Fabrication of carboxylated cellulose nanocrystal/sodium alginate hydrogel beads for adsorption of Pb(II) from aqueous solution. *Int. J. Biol. Macromol.* **2018**, *108*, 149–157. [[CrossRef](#)]
19. Shi, Y.; Liu, S.; Zhang, Z.; Liu, Y.; Pang, M. Template-free synthesis and metalation of hierarchical covalent organic framework spheres for photothermal therapy. *Chem. Commun.* **2019**, *55*, 14315–14318. [[CrossRef](#)]
20. Shi, Y.; Deng, X.; Bao, S.; Liu, B.; Liu, B.; Ma, P.; Cheng, Z.; Pang, M.; Lin, J. Self-Templated Stepwise Synthesis of Monodispersed Nanoscale Metalated Covalent Organic Polymers for In Vivo Bioimaging and Photothermal Therapy. *Chem. Asian J.* **2017**, *12*, 2183–2188. [[CrossRef](#)]
21. Yang, S.; Fu, S.; Liu, H.; Zhou, Y.; Li, X. Hydrogel Beads Based on Carboxymethyl Cellulose for Removal Heavy Metal Ions. *J. Appl. Polym. Sci.* **2011**, *119*, 1204–1210. [[CrossRef](#)]
22. Akalin, G.O.; Pulat, M. Preparation and Characterization of Nanoporous Sodium Carboxymethyl Cellulose Hydrogel Beads. *J. Nanomater.* **2018**, *2018*. [[CrossRef](#)]
23. Priyadarshi, R.; Kumar, B.; Rhim, J.W. Green and facile synthesis of carboxymethylcellulose/ZnO nanocomposite hydrogels crosslinked with Zn²⁺ ions. *Int. J. Biol. Macromol.* **2020**, *162*, 229–235. [[CrossRef](#)] [[PubMed](#)]
24. Klinpituksa, P.; Kosaiyakanon, P. Superabsorbent Polymer Based on Sodium Carboxymethyl Cellulose Grafted Polyacrylic Acid by Inverse Suspension Polymerization. *Int. J. Polym. Sci.* **2017**, 1–7. [[CrossRef](#)]
25. Cao, J.; Wang, Y.; He, C.; Kang, Y.; Zhou, J. Ionically crosslinked chitosan/poly (acrylic acid) hydrogels with high strength, toughness and antifreezing capability. *Carbohydr. Polym.* **2020**, *242*, 116420. [[CrossRef](#)]
26. Fekete, T.; Borsa, J.; Takács, E.; Wojnárovits, L. Synthesis and characterization of superabsorbent hydrogels based on hydroxyethylcellulose and acrylic acid. *Carbohydr. Polym.* **2017**, *166*, 300–308. [[CrossRef](#)]
27. Chen, Q.; Yu, H.; Wang, L.; Abdin, Z.; Yang, X.; Wang, J.; Zhou, W.; Zhang, H.; Chen, X. Synthesis and characterization of amylose grafted poly (acrylic acid) and its application in ammonia adsorption. *Carbohydr. Polym.* **2016**, *153*, 429–434. [[CrossRef](#)]
28. Kabir, S.M.F.; Sikdar, P.P.; Rahman, B.H.M.A.; Ali, B.A. Cellulose-based hydrogel materials: Chemistry, properties and their prospective applications. *Prog. Biomater.* **2018**, *7*, 153–174. [[CrossRef](#)]
29. Van Tran, V.; Park, D.; Lee, Y.C. Hydrogel applications for adsorption of contaminants in water and wastewater treatment. *Environ. Sci. Pollut. Res.* **2018**, *25*, 24569–24599. [[CrossRef](#)]
30. Castel, D.; Ricard, A.; Audebert, R.; De, L. Swelling of Anionic and Cationic Starch-Based Superabsorbents in Water and Saline Solution. *J. Appl. Polym. Sci.* **1990**, *39*, 11–29. [[CrossRef](#)]
31. Xu, Y.; Zhang, Y. Synthesis of polypyrrole/sodium carboxymethyl cellulose nanospheres with enhanced supercapacitor performance. *Mater. Lett.* **2015**, *139*, 145–148. [[CrossRef](#)]

32. Kumar, B.; Negi, Y.S. Synthesis and thermal properties of novel poly(potassium 1-hydroxy acrylate-co-potassium acrylate) based copolymer. *Mater. Lett.* **2018**, *232*, 196–201. [[CrossRef](#)]
33. Kumar, A.; Zo, S.M.; Kim, J.H.; Kim, S.C.; Han, S.S. Enhanced physical, mechanical, and cytocompatibility behavior of polyelectrolyte complex hydrogels by reinforcing halloysite nanotubes and graphene oxide. *Compos. Sci. Technol.* **2019**, *175*, 35–45. [[CrossRef](#)]
34. Miao, W.; Cheng, W.; Wang, Z.; Wang, R.; Peng, J.; Zhu, Q. Influence of n-butyl acrylate and maleic anhydride copolymer on the structure and properties of phenolic resin. *Mater. Today Commun.* **2020**, *23*, 100879. [[CrossRef](#)]
35. Kumar, B.; Negi, Y.S. Water absorption and viscosity behaviour of thermally stable novel graft copolymer of carboxymethyl cellulose and poly(sodium 1-hydroxy acrylate). *Carbohydr. Polym.* **2018**, *181*, 862–870. [[CrossRef](#)] [[PubMed](#)]
36. Chen, S.; Wu, G.; Liu, Y.; Long, D. Preparation of poly(acrylic acid) grafted multiwalled carbon nanotubes by a two-step irradiation technique. *Macromolecules* **2006**, *39*, 330–334. [[CrossRef](#)]
37. Alosmanov, R.; Imanova, J.; Wolski, K.; Ziemmermann, R.; Fiejdasz, S.; Przewoźnik, J.; Goc, K.; Kapusta, C.; Zapotoczny, S.; Szuwarzyński, M. Fabrication of functional carbon/magnetic nanocomposites as a promising model of utilization of used crosslinked polymers. *Materials* **2018**, *11*, 2595. [[CrossRef](#)]
38. Salama, A. Carboxymethyl cellulose-g-poly (acrylic acid)/calcium phosphate composite as a multifunctional hydrogel material. *Mater. Lett.* **2015**, *157*, 243–247. [[CrossRef](#)]
39. Mohy Eldin, M.S.; Omer, A.M.; Soliman, E.A.; Hassan, E.A. Superabsorbent polyacrylamide grafted carboxymethyl cellulose pH sensitive hydrogel: I. Preparation and characterization. *Desalin. Water Treat.* **2013**, *51*, 3196–3206. [[CrossRef](#)]
40. Pourjavadi, A.; Harzandi, A.M.; Hosseinzadeh, H. Modified carrageenan 3. Synthesis of a novel polysaccharide-based superabsorbent hydrogel via graft copolymerization of acrylic acid onto kappa-carrageenan in air. *Eur. Polym. J.* **2004**, *40*, 1363–1370. [[CrossRef](#)]
41. Kumar, B.; Deeba, F.; Priyadarshi, R.; Negi, Y.S. Agriculture: Super Absorbent Functional Polymers. *Encycl. Polym. Appl.* **2019**, *3*, 93–110.

Publisher's Note: MDPI stays neutral with regard to jurisdictional claims in published maps and institutional affiliations.



© 2020 by the authors. Licensee MDPI, Basel, Switzerland. This article is an open access article distributed under the terms and conditions of the Creative Commons Attribution (CC BY) license (<http://creativecommons.org/licenses/by/4.0/>).